Controlling the interaction between localized and delocalized surface plasmon modes: Experiment and numerical calculations

A. Christ,[1,2] T. Zentgraf,[1] S. G. Tikhodeev,[3] N. A. Gippius,[3] J. Kuhl,[1] and H. Giessen[4]
[1]*Max Planck Institut für Festkörperforschung, 70569 Stuttgart, Germany*
[2]*Nanophotonics and Metrology Laboratory, Swiss Federal Institute of Technology, 1015 Lausanne, Switzerland*
[3]*A. M. Prokhorov General Physics Institute RAS, Moscow 119991, Russia*
[4]*4th Physics Institute, University of Stuttgart, 70550 Stuttgart, Germany*
(Received 19 June 2006; revised manuscript received 7 September 2006; published 30 October 2006)

We study the fundamental optical effects originating from the resonant excitation of localized and delocalized surface plasmon modes supported by a multilayer metallic photonic crystal slab. The optimized model system consists of a periodic gold nanowire array and a spatially separated homogeneous silver film. We show that the spacer layer controlled dipole-surface interaction reveals a pronounced period dependence when an ordered nanowire arrangement is employed. Our analysis demonstrates that strong coupling gives rise to the formation of hybridized plasmon modes. Moreover, the magnetic activity of the metallic multilayer structure is theoretically analyzed. The presented effects provide interesting tools for the optimization of future plasmonic nanodevices and metal-based metamaterials.

DOI: 10.1103/PhysRevB.74.155435 PACS number(s): 78.66.−w, 42.70.Qs, 73.20.Mf

I. INTRODUCTION

The remarkable optical properties of metallic nanostructures have become a subject of considerable interest both from a fundamental as well as an applicational point of view.[1] Phenomena such as surface-enhanced Raman scattering,[2] the formation of plasmonic band gaps,[3] and the enhanced transmission through small apertures[4] have been widely discussed. Moreover, the realization of negative refractive index metamaterials at near infrared and optical frequencies by the appropriate design of resonant magnetic nanostructures has become the focus of recent research.[5]

Another prominent aspect is the possibility to use planar metal surfaces to modify the emission properties of a nearby layer of dipole emitters.[6] Depending on the separation distance, both radiative as well as nonradiative interaction phenomena have been reported. For example, more efficient light emitting devices are strongly believed to be a possible technical application.[7] However, especially the combination of a metal island film and a nearby conducting layer has served as an optimized model system to study the fundamental dipole-surface coupling effects. In particular, the localized plasmon resonances of a metal particle can be used as a dipolar probe.[8] As was theoretically proposed, strong frequency shifts of the particle plasmon resonances[9] and modifications of the surface plasmon dispersion have been found to depend on the barrier layer thickness.[10]

In this paper, we analyze how the light-matter interaction in presence of a partially reflecting metal surface can be further controlled when a periodic array of dipoles is introduced. This important structural modification represents a fundamental extension of previous studies and allows for direct observation of controlled coupling between localized and delocalized resonances.[11,12] We propose an entirely metallic model system, as in Refs. 9 and 13. Noble metal nanowires have been used as elementary electronic dipole oscillators within our experimental and theoretical investigations. The optical response of such nanowires in transverse magnetic (TM) polarization (magnetic field is oriented parallel to the nanowires) is generally characterized by spatially localized plasmon resonances. These are a consequence of the coherent oscillation of the conduction band electrons in the wires. In addition to these localized resonances, the periodic nature simultaneously allows for Bragg diffraction and hence enables surface plasmon excitation at the nearby silver film. Especially with regard to plasmonic band gap structures[14] or metal-clad microcavities,[15] the interplay between different plasmon modes is highly important and its dependence on the exact geometrical parameters requires a more detailed study.

II. SAMPLES AND THEORETICAL DESCRIPTION

A schematic view of the metal nanostructures is displayed in Fig. 1(a). Electron-beam lithography and a subsequent thermal evaporation step were used to fabricate the one-dimensional gold nanowire grating on top of the SiO_2 spacer layer. The dielectric barrier layer of thickness L_{sp} was deposited after the evaporation of a 20-nm-thick homogeneous silver film on top of a quartz substrate. The grating extension was restricted to $100\times100\ \mu m^2$ and the individual gold nanowire cross section of $100\times20\ nm^2$ has been kept fixed. For the numerical calculations, we employed the scattering-matrix formalism,[16] decomposing the electromagnetic field into planar waves with momenta $k_{g,x}=k_x+K_g$, $K_g=2\pi g/d_x$, $g=0,\pm1,\pm2,\ldots,\pm G$, where $k_x=\omega\sin\vartheta/c$. Here, ω is the incoming photon frequency and ϑ is the angle of incidence. The employed number of harmonics has been restricted to $N_G=2G+1=301$. The method works without any adjustable fit parameters and only the geometrical properties of the structure and the dielectric susceptibilities of the constituent materials are taken into account as input parameters.[17] However, we have to remark that an optimized gold nanowire cross section of $100\times15\ nm^2$ has been used for all scattering-matrix based calculations. This slight geometrical deviation from the experimentally obtained nanowire cross

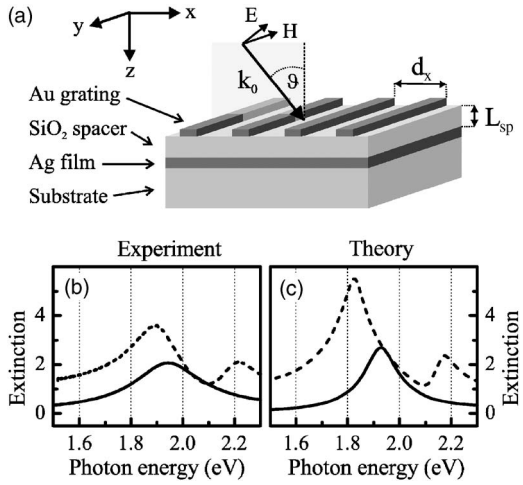

FIG. 1. (a) Schematic view of the metallic photonic crystal slab structure. The gold nanowire array and the 20-nm-thick silver film are separated by a dielectric layer of thickness L_{sp}. Experimentally and theoretically obtained extinction spectra are displayed in panels (b) and (c), respectively. Spectra of a pure gold grating (solid lines) and of a metallic multilayer structure (L_{sp}=70 nm, dashed lines) are compared. The spectra (d_x=300 nm) are shown for TM polarization and normal light incidence.

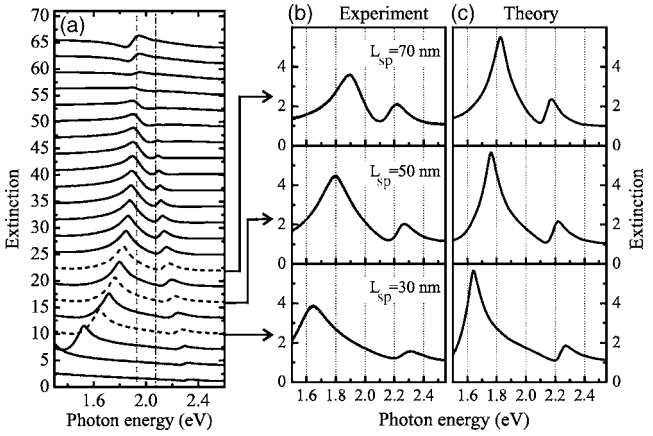

FIG. 2. (a) Calculated extinction spectra of a multilayer photonic crystal slab for TM polarization and normal light incidence. From bottom to top, the spacer layer thickness is increased from L_{sp}=0 nm (lowest spectrum) to L_{sp}=210 nm (highest spectrum) in steps of 10 nm. The grating period of d_x=300 nm is kept constant. The individual spectra are shifted upwards for clarity. The spectral positions of the supported bare modes are indicated by vertical lines (dashed line: localized particle plasmon mode, dashed-dotted line: 1st Bragg resonance of the short range surface plasmon). A direct comparison between experimental and theoretical results is given in panels (b) and (c). Structures with a spacer layer thickness of 30 nm, 50 nm, and 70 nm are studied. Spectra in panel (c) correspond to the dashed curves in panel (a).

section might be caused by uncertainties in the exact determination of the gold susceptibility.

III. SPACER LAYER DEPENDENCE

The metal film induced modifications of the nanowire extinction spectrum are highlighted in Figs. 1(b) and 1(c). The extinction spectra of a metallic multilayer structure (L_{sp} =70 nm, d_x=300 nm) are compared with results of an identical grating sample without the additional silver layer. Rather than a single localized nanowire plasmon resonance of the reference grating (solid line), two extinction maxima can be clearly observed in the case of the hybrid multilayer design (dashed line). The experimentally and theoretically observed double peak structure is a clear signature of the grating-film interaction.

The numerically obtained extinction spectra in Fig. 2(a) reveal the spacer layer dependence of the optical response. The grating-film separation is stepwise increased from L_{sp} =0 nm to L_{sp}=210 nm, while the nanowire period of d_x =300 nm is kept fixed (TM polarization, ϑ=0°). A comparison between selected experimental and theoretical results is given in Figs. 2(b) and 2(c). Overall, taking into account inhomogeneous broadening due to sample imperfections, an excellent agreement is found. The energetically lower extinction maximum in panel 2(a) can be associated with the approximate spectral position of the localized plasmon mode. Its bare energy (extracted from a calculation without introduction of the silver film) is indicated by the vertical dashed line. The strong redshift of this resonance with decreasing L_{sp} is likely due to the enhanced near-field interaction between the localized wire plasmon and its induced image when reducing the spacer layer thickness. The linear restoring forces which arise due to the collectively displaced nanowire conduction band electrons are effectively reduced. The energetically upper (and less pronounced) extinction maximum, which indicates the approximate spectral position of the first Bragg resonance of the delocalized surface plasmon, is blueshifted. The grating-induced surface mode is mainly localized at the silver-substrate interface (corresponding to a negligible thickness of the spacer layer). It is continuously converted into the short-range surface plasmon mode[18] of the symmetric film structure (corresponding to a thin silver film between quartz half spaces). Numerical simulations (not shown) reveal that the blueshift of the grating-induced surface plasmon does not appear for structures which are covered by an additional thick SiO_2 cap layer (i.e., employing a symmetric sample design). Note that the calculated position of the short-range surface plasmon mode in empty-lattice approximation (i.e., its first Bragg resonance at the Brillouin zone center) is indicated by the dashed-dotted line in Fig. 2(a).

The spectra in Fig. 2 reveal a relatively weak plasmon-plasmon interaction due to the chosen nanowire period of d_x=300 nm. In particular, the grating-induced surface plasmon resonance is spectrally detuned towards the blue with respect to the position of the localized plasmon mode. While near-field interaction dominates for small spacer layer thicknesses and directly modifies the resonance energy of the localized plasmon mode, especially the influence of radiative coupling can be further identified. For example, radiative interaction induces a so-called line shape cycle[19] and leads to a spacer layer dependent modification of the asymmetric extinction resonances of the localized mode. A characteristic situation appears for a spacer layer thickness of approxi-

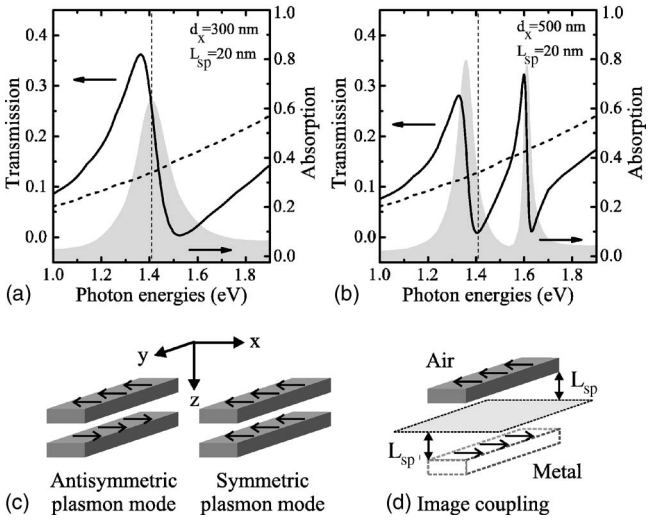

FIG. 3. Calculated transmission (solid lines) and absorption spectra (shaded area) of a multilayer photonic crystal slab structure for TM polarization and normal light incidence. Spectra for structures with a spacer layer thickness of 20 nm are shown for d_x =300 nm (a) and 500 nm (b). Additionally, the transmission spectrum of a pure 20-nm-thick silver film without nearby grating is plotted (dashed line) in both panels. The current distribution of the fundamental plasmon modes in two different coupled nanowire geometries (wire-wire or wire-image interaction) is pictorially displayed in panels (c) and (d). Note that the symmetric mode does not exist in case of image coupling.

mately 180 nm. The localized plasmon mode becomes subradiant in character when Bragg spacing is reached. In this case, the spectral signature disappears, and a relatively flat extinction spectrum is obtained.

IV. NATURE OF THE PLASMON MODES

Before we address the period- and angular-dependent optical response of the multilayer structure, it is instructive to study the physical nature of the localized plasmon mode in greater detail. Calculated transmission and absorption spectra of a multilayer structure (L_{sp}=20 nm) are shown in Figs. 3(a) and 3(b) for two different nanowire periods (d_x =300 nm and 500 nm, respectively). As a reference (dashed lines) both panels additionally include the transmission spectra of a 20-nm-thick silver film without the grating layer. In contrast to the smooth reference spectrum, the multilayer structure in panel 3(a) is characterized by a single resonance feature. The pronounced absorption maximum at 1.41 eV is directly related to a characteristic transmission resonance with a strongly asymmetric Fano-like line shape.[20] Originating from a fundamental interference phenomenon, a threefold off-resonant enhancement of the transmissivity can be observed in comparison to the plain metal layer. The pronounced resonance at 1.41 eV is itself interesting and requires further discussion. Similar to the recently discussed cut-wire pairs[21] and staple-shaped resonant magnetic nanostructures,[22] this localized plasmon mode can be interpreted in terms of a magnetic resonance.

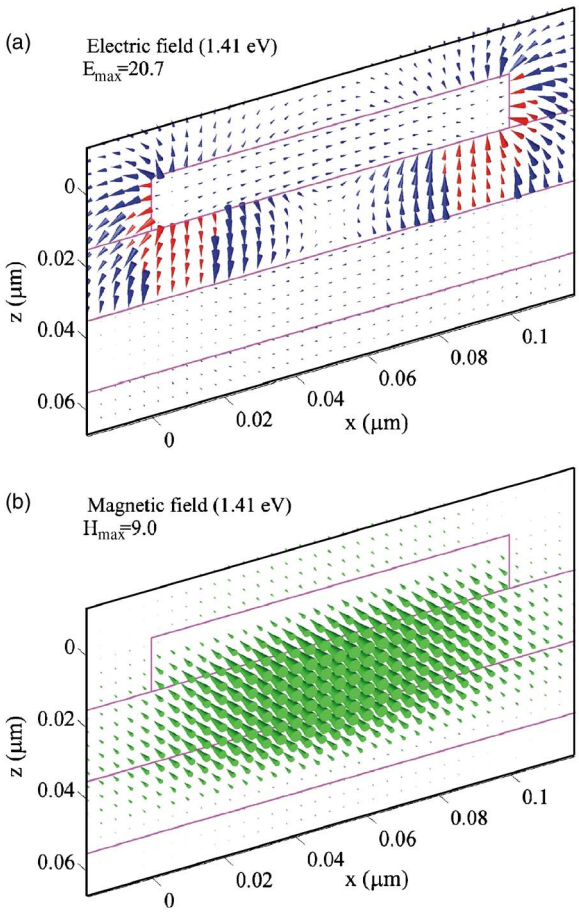

FIG. 4. (Color online) Calculated spatial distribution of the electric (a) and magnetic (b) fields in a metallic multilayer structure (TM polarization, ϑ=0°, d_x=300 nm). The fields are shown for a photon energy of $\hbar\omega$=1.41 eV [absorption maximum in Fig. 3(a)] and a spacer layer thickness of L_{sp}=20 nm. Solid magenta lines denote the cross-section of the sample structure. The length of the displayed cones is proportional to the field strength at the central point of each cone and the field direction is specified by their orientation. The red cones in panel (a) are scaled by a factor of 0.5. The field distributions are displayed for the moments of time when the field intensities (integrated over the displayed area) reach their maxima. The field magnitudes are normalized to their maximum absolute values E_{max} and H_{max} (specified in the panels) measured in units of the incoming field, respectively.

As illustrated in Figs. 3(c) and 3(d), the antisymmetric or magnetic plasmon mode of a double-wire system can be nearly mimicked by a single metal nanowire placed in close proximity to a reflecting metal surface. In a very simplified quasistatic picture, the individual gold wires in front of the silver film may be interpreted in terms of an inductor-capacitor (LC) circuit. While the inductor part is associated with the metal wire, two capacitors are formed at the wire edges. The specific nature of the related localized plasmon mode becomes immediately clear when examining the numerically obtained field distribution displayed in Fig. 4. At a photon energy of 1.41 eV (the absorption maximum), the induced circular current leads to a resonantly enhanced magnetic field within the spacer layer directly below the wires. Strong electric fields can be found at the wire edges, high-

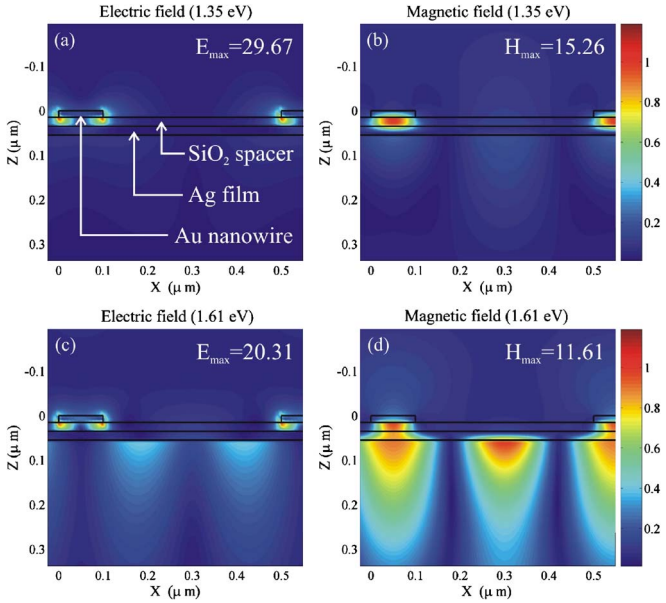

FIG. 5. (Color online) Calculated spatial field distribution of the electric and magnetic fields for normal light incidence and TM polarization. Shown are the normalized time-averaged field intensities for a nanowire structure with a periodicity of d_x=500 nm, a spacer thickness of L_{sp}=20 nm, and a 20-nm-thick silver film. The local fields are depicted for an incoming photon energy of $\hbar\omega$=1.35 eV and $\hbar\omega$=1.61 eV in a plane perpendicular to the nanowires. The chosen energies correspond to the positions of the absorption maxima in Fig. 3(b). The fields are normalized by the maximum electric ($|\vec{E}_{\max}|^2$) and magnetic field ($|\vec{H}_{\max}|^2$) intensities (specified in the panels) measured in units of the incoming field with amplitudes equal one, respectively. Black lines denote the cross section of the structure.

lighting the existing displacement currents. It is important to note that the maximum of the electric field intensities (integrated over the displayed area) is reached at approximately 1/4 of a period $T=2\pi/\omega$ earlier than the corresponding maximum of the magnetic field intensities. This indicates the standing wave character of the fields shown. Additional studies are required to clarify the effective strength of the magnetic activity and whether such a localized plasmon mode can be applied for the realization of a negative permeability at optical frequencies. For example, an experimental or theoretical determination of the complex reflection and transmission coefficients as well as near-field measurements might provide additional indirect information about the magnetic properties of the structure.

In contrast to the interaction between a discrete localized plasmon mode and a continuum of delocalized surface plasmons,[9] the *periodic* structure allows for additional control of the coupling phenomena. Figure 3(b) directly reveals the induced spectral modification due to plasmon-plasmon interaction in the ordered structure. In comparison to the short pitch grating of Fig. 3(a), where the grating-induced surface plasmon mode is found at 2.28 eV, an increased grating period of d_x=500 nm shifts the Bragg surface plasmon mode (momentum $k_{g,x}=\pm 2\pi/d_x$) nearly to resonance with the discussed localized plasmon mode. The characteristic splitting into two narrow absorption maxima can be clearly observed in Fig. 3(b) as a result of the induced polariton formation.

Additional information on the nature of the two resonances can be deduced from the corresponding electromagnetic field distributions. The calculated spatial field distributions of the electric (left panels) and magnetic (right panels) fields are displayed in Fig. 5, assuming normal light incidence and TM polarization. The normalized local fields are depicted for incoming photon energies of $\hbar\omega$=1.35 eV and $\hbar\omega$=1.61 eV in a plane perpendicular to the nanowires (i.e., xz plane). The chosen energies correspond to the spectral positions of the two absorption maxima in Fig. 3(b).

The calculated field distributions directly indicate that the two bare plasmon modes are tuned slightly off-resonance, i.e., Fig. 3(b) does not reveal the condition of maximum coupling between the localized and delocalized modes. For example, the electric and magnetic fields at a photon energy of 1.35 eV show a spatial structure similar to Fig. 4. The nature of the resonance is still strongly related to the localized surface plasmon mode. On the other hand, the spatial structures of the electric and magnetic fields at a photon energy of 1.61 eV differ substantially from the case of the lower energetic resonance. The strong evanescent field components within the substrate clearly indicate the excitation of a delocalized surface plasmon mode at the substrate metal interface. As expected, the intensity distribution of this grating-induced surface plasmon mode revels a periodicity which equals half of the grating period. However, the onset of mode mixing can already be observed. Large electric field components at the wire edges and strong magnetic fields within the spacer layer below the wires can additionally be found in Figs. 5(c) and 5(d). These components therefore indicate a partial mixing with the localized surface plasmon modes of the individual nanowires.

V. INFLUENCE OF THE GRATING PERIOD

The influence of the exact grating period and the induced modification of the spacer layer dependence are illustrated in Fig. 6. Numerically obtained contour plots are shown for grating-film structures with periods ranging from d_x =200 nm to d_x=500 nm. The spacer layer thickness is continuously increased from 0 nm to 200 nm in each panel, respectively. The spectral positions of the supported bare modes are once more indicated by horizontal lines. While the position of the localized particle plasmon of the bare nanowire grating is only weakly affected (neglecting the onset of direct near-field interaction between the individual wires for structures with $d_x \leq 200$ nm), short- and long-range surface plasmons are continuously redshifted due to a size reduction of the first Brillouin zone. The spectral positions of both surface plasmon modes of the symmetric structure (first Bragg resonance) have been calculated analytically in an empty-lattice approximation (following Ref. 18). The mirror-induced modification of the localized plasmon resonance as well as its interaction with the delocalized surface plasmon modes can be clearly observed. The increased nanowire period shifts the grating-induced plasmon modes to lower en-

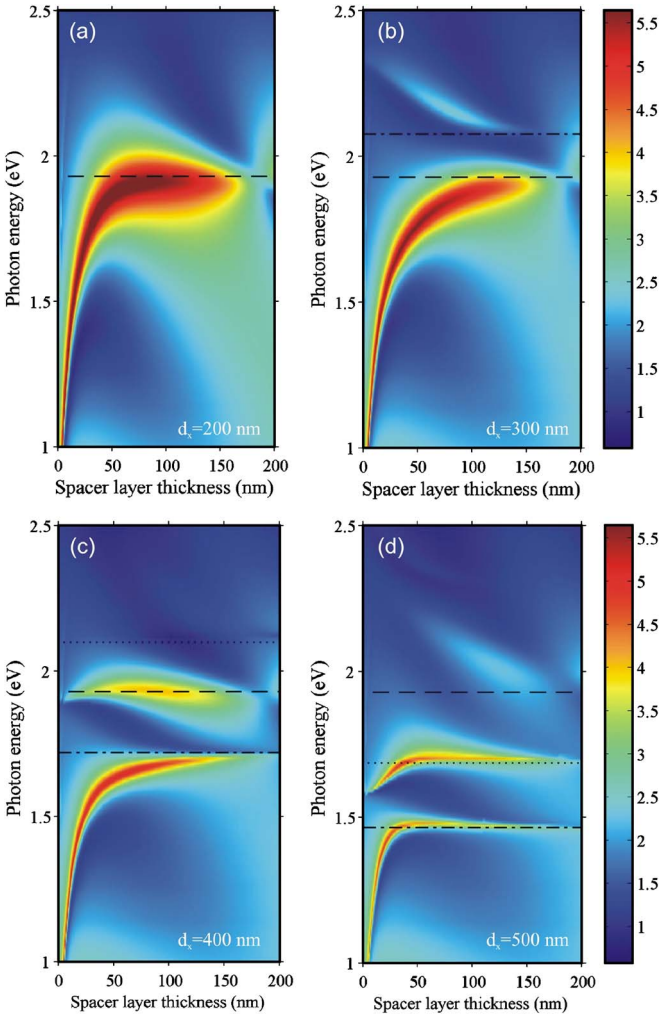

FIG. 6. (Color online) Calculated extinction contour plots of grating-film structures in dependence of the spacer layer thickness. Results for structures with $d_x=200$ nm (a), $d_x=300$ nm (b), $d_x=400$ nm (c), and $d_x=500$ nm (d) are compared. The contour plots are drawn assuming normal light incidence and TM polarization, respectively. The spectral positions of the bare modes are indicated by horizontal lines (dashed line: localized nanowire plasmon resonance, dashed-dotted line: short-range surface plasmon mode of the silver film, dotted line: long-range surface plasmon mode of the silver film).

ergies which directly results in a distinct anticrossing behavior.

Figure 6(a) displays the spacer layer dependence of the localized nanowire plasmon mode for the case of strongly detuned grating-induced surface plasmon resonances. The spectra clearly indicate the spectral modifications due to near-field interaction and radiative coupling. The extinction maxima indicate the polariton dispersion, whereas the dashed horizontal line at 1.9 eV shows the dispersion of the bare localized plasmon mode. The contour map in Fig. 6(b) provides a more detailed overview of the dependencies displayed in Fig. 2. The grating period of $d_x=300$ nm introduces only a very weak plasmon-plasmon interaction which mainly affects the spectral width of the nanowire assigned localized mode. More dramatic changes of the optical response are depicted in Fig. 6(c), i.e., when the localized plasmon is spectrally located in between the positions of the bare short- and long-range modes. The redshifted particle plasmon resonance approaches the spectral position of the short-range mode when increasing the spacer layer thickness. On the other hand, the short-range surface plasmon shows a flat dispersion and merges with the localized mode. Strong coupling, therefore, results in a mode mixing (i.e., *polariton formation*) for intermediate grating-film separations. The most significant modifications, however, are observed for a sample structure with a grating period of $d_x=500$ nm. Now the localized plasmon resonance interacts with *both* short- and long-range surface plasmon modes *simultaneously*. The numerically obtained contour plot reveals two spectrally narrow lines which are characterized by a flat dispersion. The near-field induced redshift is only visible for small grating-film separations due to the arising anticrossing behavior. Note that the observed strong coupling phenomena are, in general, directly related to the recently discovered waveguide-plasmon polariton formation in metallo-dielectric photonic crystal slab structures (considering the replacement of the dielectric waveguide by a metallic one).[23]

VI. DISPERSION

We now examine the angular dependent dispersion of the plasmon modes to strengthen our previous interpretations. This analysis allows for precise determination of the polariton band structure close to the center of the first Brillouin zone and helps in assigning the contributing modes. A direct comparison of the experimental and theoretical results for TM polarization can be found in Figs. 7(a) and 7(b). Extinction spectra for a multilayer structure with a 70-nm-thick spacer layer are plotted. From bottom to top, the angle of incidence is increased in steps of 6° while the nanowire period of $d_x=300$ nm remains constant. Additionally, a more detailed contour map of the numerically obtained extinction spectra is displayed in Fig. 7(c). As the incidence angle is increased ($\vartheta>0°$), a clear splitting into three resonances and a gradual shift of the arising extinction maxima is observed.

The displayed angular dependence can be understood considering the dispersion of the grating-induced plasmon mode. The calculated dispersion of the short-range surface plasmon of a 20-nm-thick silver layer (i.e., a film between quartz half spaces) is shown in Fig. 7(d) in empty-lattice approximation. In contrast to this simplified approximation, the degeneracy of the grating-induced surface plasmon mode folded into the first Brillouin zone is generally lifted at the zone center ($k_x=0$). The arising band edge states are characterized by a reverse symmetry. Similar to quasiguided modes of dielectric slab waveguides,[24] spectrally separated symmetric (i.e., radiant) and antisymmetric (i.e., subradiant) surface plasmon modes exist at the zone center.[25] However, the supported antisymmetric surface plasmon mode can be optically excited only for inclined illumination. Measurements under oblique incidence therefore reveal a characteristic mixing between a single localized mode and two extended surface plasmon modes of opposite symmetry. An important further

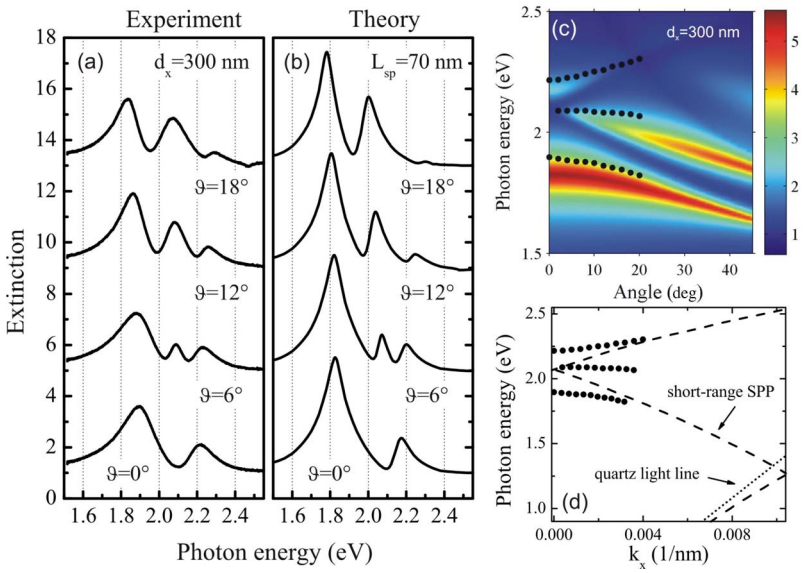

FIG. 7. (Color online) Measured (a) and calculated (b) extinction spectra of the multilayer metallic photonic crystal (d_x=300 nm, L_{sp}=70 nm, TM polarization) in dependence of the incidence angle. The angle ϑ is increased from 0° to 18° in steps of 6°. The individual spectra are shifted upwards for clarity. Additionally, the numerically obtained extinction contour plot of the studied structure is depicted in panel (c). The dispersion of the short-range surface plasmon mode in empty-lattice approximation (dashed line) is shown in panel (d). The experimentally obtained positions of the extinction maxima are indicated by solid circles, respectively.

observation is the reduced excitation efficiency of the upper blueshifted surface plasmon mode for nonzero incidence angles. The displayed spectra thus clearly prove that the grating-induced surface plasmon modes are strongly enhanced due to mode mixing in the presence of the localized resonance. A related fundamental question, namely the spacer layer dependent bandwidth of the arising plasmonic stopband in the vicinity of the localized plasmon mode, will be addressed in a forthcoming paper.

VII. DISORDER

Finally, the influence of random defects, i.e., the deviation from perfect Bragg periodicity is probed experimentally. This interesting approach allows for additional control of the coupling phenomena.[26] For example, the excitation of the grating-induced surface plasmon mode is prevented in case of a random nanowire arrangement and only the localized plasmon resonance should be observable. Similar to Ref. 27, where the structure factor of a photonic crystal superlattice was modified continuously, artificial disorder is introduced during electron beam lithography. The spatial positions of the individual grating wires are generally varied randomly within a certain range around the original grid positions. The wire displacement is pictorially displayed in Fig. 8(b). The implemented deviation Δr_i of the ith nanowire is determined by $\Delta r_i = f R_i$. Here, f is a weighting factor and R_i is a randomly chosen distance. R_i is however limited to the interval $\pm d_x/2$ to avoid crossing of the neighboring nanowires. All distances within the specified interval are selected with equal probability. Note that a new set of R_i values is chosen for each weighting factor f.

The experimental results for a gold nanowire structure with a grating period of d_x=400 nm, a silver film thickness of h_{film}=20 nm, and a spacer layer thickness of L_z=50 nm are shown in Fig. 8(a). All extinction spectra are displayed for normal light incidence and TM polarization. From top to bottom, the amount of disorder (specified by the displayed weighting factor f) is continuously increased. Additionally, the calculated spectrum of a periodic structure is depicted as a reference (dotted line). A gold nanowire cross section of 90×15 nm^2, a grating-film separation of L_z=50 nm, a silver film thickness of h_{film}=20 nm, and a period of d_x=400 nm have been used for the numerical simulations to obtain excellent agreement with the measured spectrum (f=0). The interaction between the localized nanowire and the grating induced surface plasmon modes results in two pronounced spectral peaks in case of perfect periodicity. As discussed before, these two resonances can be directly related to the branches of the arising polariton mode. Increasing disorder however leads to characteristic modifications of the extinction spectra. Spectral shifts as well as an attenuation of the maxima can be observed. In case of large disorder, i.e., assuming a weighting factor f=1, only a single spectrally broad extinction maximum remains visible.

The observations can be simply explained by the reduced excitation efficiency of the involved grating induced surface plasmon mode. It is well known that the coupling between the incident light field and the bare surface plasmon mode is directly proportional to the absolute value of the Fourier component of the grating with spatial frequency $g_x = 2\pi/d_x$. A Fourier decomposition of the investigated lattice geometries and the resulting amplitudes of the spatial harmonics can be found in Fig. 8(c). An increased disorder generally results in an attenuation of the amplitude of the corresponding Fourier component and thus in a lowering of the surface plasmon excitation efficiency. Therefore also the polariton formation is suppressed by higher amounts of disorder. The reduced excitation efficiency leads to a weakening of the effective interaction between the localized and the grating induced surface plasmon modes. In the limit f=1, the excitation efficiency of the grating-induced surface plasmon approaches zero. Only the bare nanowire plasmon resonance, which does not require periodicity for optical excitation, can be observed in the measured extinction spectra for structures with $f \geq 0.8$. However, although the localized wire plasmon resonances can still be excited, their linewidth and spectral position is strongly affected by the disorder. An increased

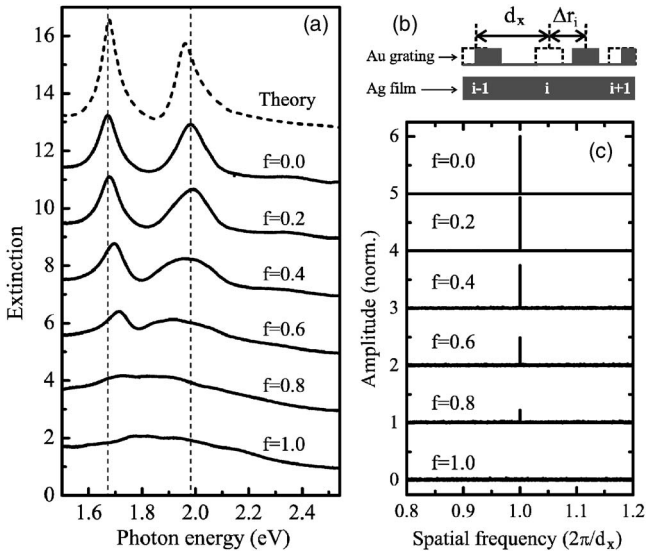

FIG. 8. (a) Experimentally measured extinction spectra of grating-film structures with $L_{sp}=50$ nm for normal light incidence and TM polarization. Starting from a perfectly periodic structure with $d_x=400$ nm ($f=0.0$), random defects in the position of the nanowires were introduced from $f=0.0$ ($\Delta r_{max}=0$ nm) to $f=1.0$ ($\Delta r_{max}=\pm 200$ nm) in steps of 0.2. Additionally, the numerically obtained extinction spectra of a periodic structure without defects is plotted as a reference (dashed line). A schematic view of the grating-film structure is shown in panel (b). The dotted squares mark the cross section of the original wire positions without displacement. The parameter Δr_i indicates the spatial shift of the ith nanowire. The Fourier decompositions of the grating structures in dependence of the spatial frequency and of the weighting factor f are displayed in panel (c). Note that the spectra in panels (a) and (b) are shifted upwards for clarity.

disorder may result in the formation of nanowire pairs that exhibit very small interparticle spacings. In such a case, near-field coupling will induce a redshift and broadening of the collective dimer plasmon mode. In the worst case, even a direct spatial overlap of the nanowires might be possible. In addition to appearing proximity effects during electron beam writing, both effects generally lead to an increased inhomogeneous broadening of the detected nanowire plasmon resonances. In particular, such an inhomogeneous broadening of the localized plasmon resonance can be clearly observed for the bottom-most extinction spectra of Fig. 8. Thus, our investigation clearly demonstrates that we can switch from a polaritonic system (i.e., coupled surface plasmon modes) to a system which only features localized particle plasmon modes by simply destroying the periodicity of the lattice.

VIII. CONCLUSION

In summary, we have analyzed the coupling between localized and delocalized surface plasmon resonances in a multilayer metallic photonic crystal slab. The experimental and theoretical spectra reveal a mixing of the supported modes due to polariton formation. A clear period-dependent as well as angle-dependent anticrossing behavior is observed as a result of mode coupling. Furthermore, the magnetic properties of the proposed sample design are discussed theoretically. The presented phenomena are especially important with regard to future plasmon engineering and the design of novel metamaterials.

ACKNOWLEDGMENTS

This work was financially supported by the German Federal Ministry of Education and Research (Grant No. FKZ 13N8340/1), the Deutsche Forschungsgemeinschaft (Priority Program Contracts No. SPP1113 and No. FOR557), the Russian Academy of Sciences, the Russian Ministry of Education and Science (Contract No. 02.442.11.7410), the Russian Foundation for Basic Research (Grant No. 06-02-17211), and the European Commission (Grant No. FP6-2002-IST-1-507879). The authors acknowledge the support of K. von Klitzing and O. J. F. Martin and thank T. Meyrath for critical reading of the manuscript.

[1] W. L. Barnes, A. Dereux, and T. W. Ebbesen, Nature (London) **424**, 824 (2003).
[2] M. Moskovits, Rev. Mod. Phys. **57**, 783 (1985).
[3] S. C. Kitson, W. L. Barnes, and J. R. Sambles, Phys. Rev. Lett. **77**, 2670 (1996).
[4] T. W. Ebbesen, H. J. Lezec, H. F. Ghaemi, T. Thio, and P. A. Wolff, Nature (London) **391**, 667 (1998).
[5] S. Linden, C. Enkrich, M. Wegener, J. Zhou, T. Koschny, and C. M. Soukoulis, Science **306**, 1351 (2004).
[6] W. L. Barnes, J. Mod. Opt. **445**, 661 (1998).
[7] K. Okamoto, I. Niki, A. Shvartser, Y. Narukawa, T. Mukai, and A. Scherer, Nat. Mater. **3**, 601 (2004).
[8] B. C. Buchler, T. Kalkbrenner, C. Hettich, and V. Sandoghdar, Phys. Rev. Lett. **95**, 063003 (2005).
[9] W. R. Holland and D. G. Hall, Phys. Rev. Lett. **52**, 1041 (1984).
[10] W. R. Holland and D. G. Hall, Phys. Rev. B **27**, 7765 (1983).
[11] T. A. Kelf, Y. Sugawara, J. J. Baumberg, M. Abdelsalam, and P. N. Bartlett, Phys. Rev. Lett. **95**, 116802 (2005).
[12] J. Cesario, R. Quidant, G. Badenes, and S. Enoch, Opt. Lett. **30**, 3404 (2005).
[13] T. Kume, N. Nakagawa, S. Hayashi, and K. Yamamoto, Solid State Commun. **93**, 171 (1995).
[14] S. I. Bozhevolnyi, J. Erland, K. Leosson, P. M. W. Skovgaard, and J. M. Hvam, Phys. Rev. Lett. **86**, 3008 (2001).
[15] A. P. Hibbins, W. A. Murray, J. Tyler, S. Wedge, W. L. Barnes, and J. R. Sambles, Phys. Rev. B **74**, 073408 (2006).
[16] S. G. Tikhodeev, A. L. Yablonskii, E. A. Muljarov, N. A. Gippius, and T. Ishihara, Phys. Rev. B **66**, 045102 (2002).
[17] P. B. Johnson and R. W. Christy, Phys. Rev. B **6**, 4370 (1972).
[18] J. J. Burke, G. I. Stegeman, and T. Tamir, Phys. Rev. B **33**, 5186 (1986).
[19] X. L. Zheng, D. Heiman, B. Lax, and F. A. Chambers, Appl.

Phys. Lett. **52**, 287 (1988).
[20] U. Fano, Phys. Rev. **124**, 1866 (1961).
[21] G. Dolling, C. Enkrich, M. Wegener, J. F. Zhou, C. M. Soukoulis, and S. Linden, Opt. Lett. **30**, 3198 (2005).
[22] S. Zhang, W. Fan, B. K. Minhas, A. Frauenglass, K. J. Malloy, and S. R. J. Brueck, Phys. Rev. Lett. **94**, 037402 (2005).
[23] A. Christ, S. G. Tikhodeev, N. A. Gippius, J. Kuhl, and H. Giessen, Phys. Rev. Lett. **91**, 183901 (2003).
[24] A. Christ, T. Zentgraf, J. Kuhl, S. G. Tikhodeev, N. A. Gippius, and H. Giessen, Phys. Rev. B **70**, 125113 (2004).
[25] C. Ropers, D. J. Park, G. Stibenz, G. Steinmeyer, J. Kim, D. S. Kim, and C. Lienau, Phys. Rev. Lett. **94**, 113901 (2005).
[26] D. Nau, A. Schönhardt, C. Bauer, A. Christ, T. Zentgraf, J. Kuhl, and H. Giessen, Phys. Status Solidi B **10**, 2331 (2006).
[27] T. Zentgraf, A. Christ, J. Kuhl, N. A. Gippius, S. G. Tikhodeev, D. Nau, and H. Giessen, Phys. Rev. B **73**, 115103 (2006).